

Impurities block the α to ω martensitic transformation in titanium

R. G. Hennig¹, D. R. Trinkle¹, J. Bouchet², S. G. Srinivasan², R. C. Albers², and J. W. Wilkins¹

¹*Department of Physics, Ohio State University, Columbus, OH 43210*

²*Los Alamos National Laboratory, Los Alamos, NM 87545*

(Dated: September 28, 2018)

The onset and kinetics of martensitic transformations are controlled by impurities trapped during the transformation. For the $\alpha \rightarrow \omega$ transformation in Ti, *ab initio* methods yield the changes in both the *relative stability* of and *energy barrier* between the phases. Using the recently discovered transformation pathway, we study interstitial O, N, C; substitutional Al and V; and Ti interstitials and vacancies. The resulting microscopic picture explains the observations, specifically the suppression of the transformation in A-70 and Ti-6Al-4V titanium alloys.

PACS numbers:

Impurities control the onset and kinetics of martensitic phase transformations—diffusionless structural transformations proceeding near the speed of sound [1]. The abundant use of martensitic materials in engineering technologies is not underpinned by a microscopic understanding of the effects of impurities during the transformation. The $\alpha \rightarrow \omega$ martensitic transformation in Ti lowers its toughness and ductility, affecting its use in the aerospace industry. The 2 to 9 GPa range in the published transition pressures of nominally pure Ti [2, 3] is believed to be caused by sample purity [4, 5]. Systematic studies show a large sensitivity to small amounts of impurities [6, 7]. Two commercial Ti alloys—A-70 and Ti-6Al-4V—show no transformation up to 35 GPa [7].

Impurities pose two theoretical challenges: The effect on the *relative stability* of the two phases and the *energy barrier* of the transformation. Understanding both of these requires the atomistic pathway for $\alpha \rightarrow \omega$ to model the impurity motion during the transformation. The near sonic speed of the transition prohibits diffusion during the transformation, thus requiring impurities to move collectively with their local environment. Recently Trinkle *et al.* identified from all possible transformation pathways the $\alpha \rightarrow \omega$ mechanism with the lowest energy barrier of 9 meV/atom.

This paper exploits this fast transformation that traps the impurities in their known path to systematically study a range of impurities, including those in the commercial Ti alloys A-70 and Ti-6Al-4V. (1) We study interstitial O, N, C; substitutional Al and V; Ti interstitials and vacancies. These impurities and defects affect the transformation by shifting the relative stability of and energy barrier between the α and ω phases. (2) Interstitial impurity effects are governed primarily by their size, while substitutional impurities affect the transformation by changing the *d*-electron concentration. (3) The most important impurities, O in A-70 Ti and Al in Ti-6Al-4V, more than double the transition barrier and increase the energy of ω relative to α , explaining the observed suppression of the $\alpha \rightarrow \omega$ transition.

Method – The *ab initio* calculations are performed with

VASP [8, 9], a density functional code using a plane-wave basis and ultrasoft Vanderbilt type pseudopotentials [10, 11]. The generalized gradient approximation of Perdew and Wang is used [12]. A plane-wave kinetic-energy cutoff of 400 eV ensures energy convergence to 1 meV/atom. The k-point meshes for the different structures are chosen to guarantee the same accuracy. To avoid unphysical short distances between the atoms, it is necessary to include the Ti *3p* states as valence states in addition to the usual *4s* and *3d* states. For the other elements the pseudopotentials describe the core states as follows: V [Ar], Al [Ne], O, N and C [He].

Impurity locations and formation energies are determined by relaxations using $4 \times 4 \times 3$ and $3 \times 3 \times 4$ supercells for the α and ω phases with 96 and 108 atoms, respectively. This results in a 1% impurity concentration. A $2 \times 2 \times 2$ k-point mesh is used. The atom positions are relaxed until the total energy changes by less than 1 meV, corresponding to atomic-level forces $F_{\max} \leq 20$ meV/Å. Altogether this provides an energy accuracy of 0.5 meV/atom.

NEB calculations with variable cell shape at constant pressure yield the energy barriers of the martensitic transformation [13]. The pathway is represented by 18 intermediate images of a 48 Ti atom supercell constructed using $\sqrt{2} \times 2\sqrt{2} \times 2$ cells of the TAO-1 mechanism with a $4 \times 4 \times 4$ k-point mesh. This results in an impurity concentration of 2%. Comparing the formation energies for the 48 atom supercell with the larger cells of 96 and 108 atoms provides an estimate of the finite size error of 0.05 eV. The images are relaxed until the energy of each image changes by less than 1 meV, corresponding to atomic-level forces $F_{\max} \leq 50$ meV/Å and stresses $\sigma_{\max} \leq 20$ MPa. Altogether this yields an energy barrier accuracy of 1 meV/atom, the same as the finite size error. To compare the effects of different defects, all energy barriers are reported relative to the α structure for that defect, and in units of meV per 48 Ti atoms.

Interstitial impurities – Figure 1 shows the location of interstitial impurities and the effect of the transformation on these sites. The interstitial impurity sites were found

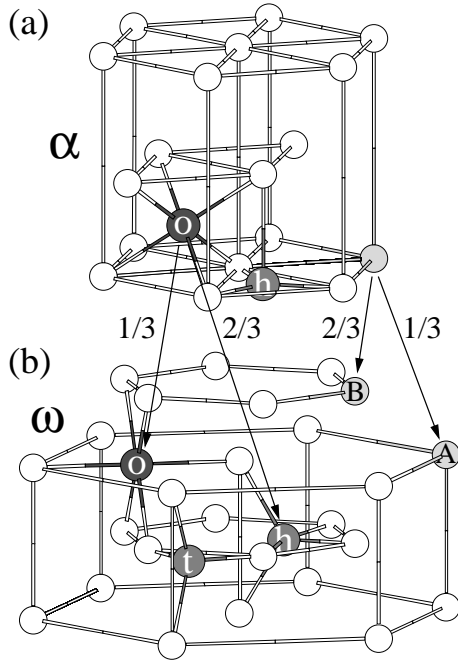


FIG. 1: Octahedral (o), tetrahedral (t), and hexahedral (h) sites for interstitial impurities as well as A and B sites for substitutional impurities in the α and ω phases. The α and ω phases each contain one unique o, t, and h site. The α_{tet} site relaxes to the nearby α_{hex} site for all three impurities (O, N, C). The hexahedral site is a distorted double-tetrahedral site with five neighbors. The arrows indicate the transformation of the impurity and lattice sites in the TAO-1 mechanism, and the relative proportions.

by placing O, N, and C impurities on all interstitial sites in α and ω and relaxing the atomic positions. Each phase contains one unique octahedral, tetrahedral, and hexahedral site. However, the tetrahedral site in α is unstable for O, N, and C and relaxes to the nearby hexahedral site in the basal plane. The “hexahedral” site is a distorted double-tetrahedral site with five neighbors, formed by a triangle of the basal plane and the two atoms right above and below the center of the triangle. The instability of the tetrahedral site is unexpected from crystallographic considerations [14] and is due to atomic relaxations. In ω the tetrahedral and hexahedral sites are both stable, and they are close in energy and location.

Table I(a) shows the formation energies of the interstitial defects in α and ω . The energy is measured relative to molecular O_2 , N_2 and graphite, respectively. For both α and ω the octahedral site is more stable than the tetrahedral or hexahedral sites. This is simply related to the size of the interstitial sites: larger sites have lower formation energies. Comparison between the α and ω interstitial impurities shows that the octahedral formation energy is slightly lower for α ; this difference shifts the relative energy of the two crystal structures, decreasing the stability of ω over α .

Figures 2(a) and (b) show octahedral sites in α —favored by O, N, and C—transforming into two possible sites in ω and increase the energy barrier for the transformation. The TAO-1 pathway breaks the hexagonal symmetry and transforms a third of the octahedral sites into the ω octahedral site and two thirds into the ω hexahedral site. The presence of impurities increases the energy barrier regardless of the final site of the impurities; however, this increase is much larger for the octahedral to hexahedral pathway than for the octahedral to octahedral one. For all three impurities, despite their different chemistry, their similar size results in nearly identical barriers.

TABLE I: Formation energies and location of interstitial and substitutional impurities as well as vacancies and self-interstitials in the α ($P6_3/mmc$) and ω ($P6/mmm$) phases. The formation energies E_f for O, N, and C are measured relative to molecular O_2 , N_2 , and graphite, respectively, and for Al and V relative to their fcc and bcc phase, respectively. For the vacancies and self-interstitials the formation energies are measured relative to the corresponding α or ω phases. All calculations are performed at 1 at.% defect concentration. For each site, the average nearest neighbor distance after relaxation, R_{NN} , is similar for all impurities; hence, we show the range of values. The coordination number Z at each site is also listed.

Site	Wyckoff pos. ^a	R_{NN} [Å]	Z	E_f [eV]		
(a) <i>Interstitial impurities</i>				O	N	C
α_{oct}	2(a) (0,0,0)	2.06–2.09	6	−6.12	−5.10	−1.58
α_{hex}	2(d) ($\frac{2}{3}, \frac{1}{3}, \frac{1}{4}$)	1.91–1.95	5	−4.93	−3.41	+0.49
ω_{oct}	3(f) ($\frac{1}{2}, 0, 0$)	2.03–2.17	6	−6.06	−4.99	−1.36
ω_{hex}	6(k) ($x, 0, \frac{1}{2}$)	1.92–2.18	5	−4.47	−3.03	+0.61
ω_{tet}	6(m) ($x, 2x, \frac{1}{2}$)	1.90–2.02	4	−4.38	−2.83	+0.78
(b) <i>Substitutional impurities</i>				Al	V	
α	2(c) ($\frac{1}{3}, \frac{2}{3}, \frac{1}{4}$)	2.85–2.92	12	−0.88	+0.51	
ω_A	1(a) (0,0,0)	2.82–3.00	14	−0.90	+0.60	
ω_B	2(d) ($\frac{1}{3}, \frac{2}{3}, \frac{1}{2}$)	2.60–3.00	11	−0.47	+0.33	
(c) <i>Vacancy</i>						
α	2(c) ($\frac{1}{3}, \frac{2}{3}, \frac{1}{4}$)	2.85–2.94	12		+2.03	
ω_A	1(a) (0,0,0)	2.83–3.02	14		+2.92	
ω_B	2(d) ($\frac{1}{3}, \frac{2}{3}, \frac{1}{2}$)	2.12–3.03	11		+1.57	
(d) <i>Self-interstitial</i>						
α_{oct}	2(a) (0,0,0)	2.47	6		+2.58	
α_{dumb}	2(d) ($\frac{2}{3}, \frac{1}{3}, \frac{1}{4}$)	2.05	1		+2.87	
ω_{oct}	3(f) ($\frac{1}{2}, 0, 0$)	2.33–2.60	6		+3.76	
ω_{hex}	6(k) ($x, 0, \frac{1}{2}$)	2.21–2.55	5		+3.49	
ω_{tet}	6(m) ($x, 2x, \frac{1}{2}$)	2.15–2.51	4		+3.50	

^aSee Ref. 15

Substitutional impurities – Table I(b) shows the formation energies of the substitutional Al and V for α and the A and B sites in ω . These energies are defined relative to fcc Al and bcc V. Comparison between the α and ω substitutional impurities shows that, for both Al and V, the favored ω site is lower than the α site. However,

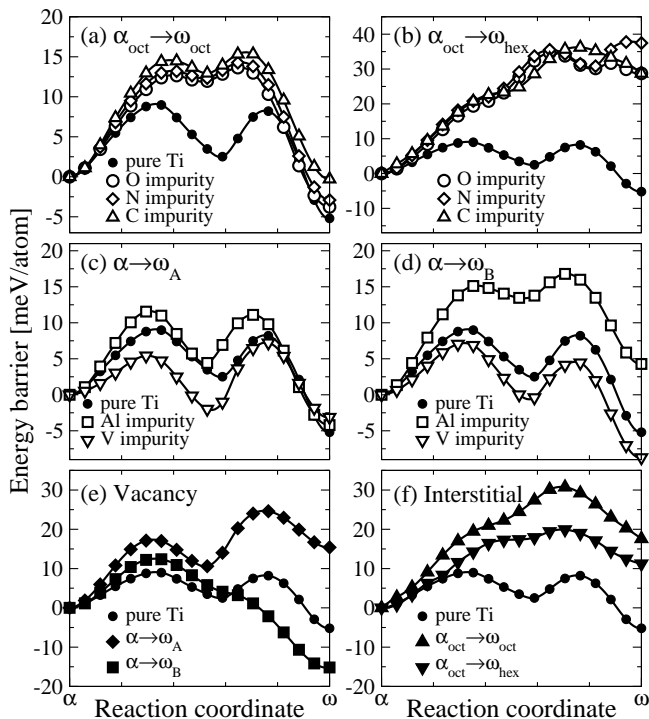


FIG. 2: Energy barrier for the TAO-1 mappings of interstitial and substitutional impurities, as well as vacancies and interstitials in Ti relative to the α phase. The defect concentration is 2%. The endpoint energies match the formation energies of Table I for a defect concentration of 1 at.% within 1 meV/atom, providing an accuracy estimate for the barrier. The interstitial O, N, and C impurities occupy the octahedral sites in α and transform either (a) into the octahedral site in ω or (b) into the hexahedral site, with a 1 : 2 relative ratio. The substitutional Al and V impurities transform in ω either (c) to the A site or (d) to the B site, with a 1 : 2 relative ratio. Figure (e) shows the barrier for vacancies and (f) for the Ti-interstitial defects. The vacancy transforms from the α sites to the A and B sites in ω with a ratio of 1 : 2. The interstitial transforms from the octahedral site in α to the octahedral and hexahedral sites in ω , also with a ratio of 1 : 2.

during the transformation, a random mixture of ω occupations will be produced in a 1 : 2 ratio as shown in Figure 1. In that case, the formation energy combination $\omega_A/3 + 2\omega_B/3$ is *lower* than α for V, and *higher* for Al. This is expected to *increase* the stability of ω relative to α with V, and *decrease* the stability of ω with Al.

Figure 2(c) and (d) show how the α substitutional sites for Al and V transform to the two possible ω sites and effect the transformation barrier. The TAO-1 pathway lowers the symmetry and transforms a third of the α sites into ω_A sites and two thirds into ω_B sites. The presence of impurities changes the energy barrier in a similar fashion as the formation energies. Since the shift in the barrier matches the shift in the relative energies of α and ω , we conclude it is due to the d -electron concentration. The d -electron effect is also seen in the alloying behavior: Transition metals with large d -electron con-

centrations such as V, Mo, Fe, Ta stabilize the ω phase, while simple metals and early transition metals such as Al favor α [4].

Titanium vacancies and interstitials – Table I(c) and (d) show the formation energies of the vacancies and Ti-interstitial defects in α and ω , respectively. The reference energy is the appropriate Ti crystal phase. For the vacancies, the ω_B site—which relaxes the 6-fold B-sublattice rings into 5-fold rings—is most forgiving. However, during the transformation, a random mixture of ω occupations will be produced in a 1 : 2 ratio; in that case, the formation energy combination $\omega_A/3 + 2\omega_B/3$ is nearly identical to the α vacancy. The interstitials are energetically favorable, as is expected for a closed-packed metal. While the α -octahedral site has the lowest formation energy, there is an energetically close defect formed when the tetrahedral interstitial relaxes and forms a [0001] dumbbell configuration. All the ω interstitial sites are nearly degenerate in energy. The increased formation energy for ω interstitials over α interstitials is expected to shift the relative energy of the two crystal structures, decreasing the stability of ω over α .

Figure 2(e) and (f) show how vacancies and Ti-interstitials transform to two possible sites in ω and increase the energy barrier for the transformation. The TAO-1 pathway acts on vacancies and Ti-interstitials as for substitutional and interstitial impurities, respectively. The presence of vacancies increases the barrier in both cases, though the effect is much more pronounced when transforming to the ω_A vacancy. The presence of interstitials increases the energy barrier regardless of the final site of the interstitial; unlike the impurities, there is not much difference between the octahedral and hexahedral pathways. Due to their inherently low concentration the self defects will not have any significant effect on the transformation.

Discussion – The α - ω phase transition is sensitive to small energy changes. At zero pressure and temperature, the ω phase is about 4 meV/atom lower in energy than α [16] and the energy barrier from α to ω is 9 meV/atom [17]. It takes 10 GPa to overcome the energy barrier in shock experiments [7] or 280 K to overcome the energy difference [18]. Hence, we expect a significant change in transition temperature and pressure due to the energy shift caused by impurities.

Table II shows the effect of impurities in A-70 Ti and Ti-6Al-4V, especially the significant effect of O and Al. Overall, we find the presence of impurities in both alloys suppresses the $\alpha \rightarrow \omega$ martensitic phase transition by increasing both the ω energy relative to α and the energy barrier. The increased energy barrier is expected to reduce nucleation and to slow down the transformation. The change of the α - ω energy difference shifts the α - ω phase boundary [18] downward by several hundred degrees and thus at room temperature increases the transformation pressure dramatically.

TABLE II: Change of the relative energy between α and ω and of the energy barrier by impurities in the A-70 and the Ti-6Al-4V alloys. The impurity concentrations are taken from Ref. 7.

Alloy	Impurity	$\Delta E_{\omega-\alpha}$ [meV]	ΔE_b [meV]
A-70:	O (1.10 at.%)	+12	+10
	N (0.08 at.%)	+1	+1
	C (0.07 at.%)	+1	+1
	Total	+14	+12
Ti-6Al-4V:	Al (10.7 at.%)	+29	+31
	V (3.8 at.%)	-3	-3
	O (0.5 at.%)	+6	+5
	Total	+33	+33

The other interstitial impurities, N and C, have an effect similar to O. Despite their different chemistry, all increase the energy barrier and the relative energy by nearly the same amount. This indicates the primary effect is steric, and hence, we expect other interstitials of comparable size to have similar effects. In the A-70 Ti and Ti-6Al-4V alloys the effect of N and C is smaller proportional to their lower concentration.

In contrast, the substitutional Al and V impurities have opposite effects due to the change in d -electron concentration. As expected from the alloying behavior of Ti [4], V decreases the energy of ω and Al increases it. We observe the same behavior for the energy barriers. The Al impurity reduces the d -electron concentration by two, while V increases it by one; thus Al has a larger effect on the $\alpha \rightarrow \omega$ transformation. Commercial Ti-6Al-4V alloy contains both; however, the concentration of Al (11 at.%) is three times higher than the concentration of V (4 at.%), explaining the observed suppression of the $\alpha \rightarrow \omega$ transformation.

Conclusion – We determined the energy and location of point defects in α and ω Ti and showed how they suppress the martensitic transformation. Interstitial O, N, and C occupy the octahedral interstitial sites in α and ω and transform into the octahedral and hexahedral interstitial sites in ω . The interstitial impurities retard the transformation by increasing the transformation energy barrier while the substitutional impurities Al and V influence the barrier by changing the d -electron concen-

tration. The effect of impurities on relative energies and energy barriers is central to understanding martensitic transformations.

This work was supported by NSF and DOE. Computational resources were provided by the Ohio Supercomputing Center and NERSC. We thank G. T. Gray for helpful discussions.

-
- [1] G. B. Olson and W. S. Owen, eds., *Martensite* (ASM, Metals Park, OH, 1992).
 - [2] A. Jayaraman, J. W. Klement, and G. C. Kennedy, Phys. Rev. **131**, 644 (1963).
 - [3] V. A. Zilbershtein, N. P. Chistotina, A. A. Zharov, N. A. Grishina, and E. I. Estrin, Fiz. Met. Metalloved. **39**, 445 (1975).
 - [4] S. K. Sikka, Y. K. Vohra, and R. Chidambaram, Prog. Mater. Sci. **27**, 245 (1982).
 - [5] C. W. Greeff, D. R. Trinkle, and R. C. Albers, J. Appl. Phys. **90**, 2221 (2001).
 - [6] Y. K. Vohra, S. K. Sikka, S. N. Vaidya, and R. Chidambaram, J. Phys. Chem. Solids **38**, 1293 (1977).
 - [7] G. T. Gray, C. E. Morris, and A. C. Lawson, in *Titanium '92: Science and Technology*, edited by F. H. Froes and I. L. Caplan (TMS, Warrendale, PA, 1993), p. 225.
 - [8] G. Kresse and J. Hafner, Phys. Rev. B **47**, 558 (1993).
 - [9] G. Kresse and J. Furthmüller, Phys. Rev. B **54**, 11169 (1996).
 - [10] D. Vanderbilt, Phys. Rev. B **41**, 7892 (1990).
 - [11] G. Kresse and J. Hafner, Journal of Physics: Condensed Matter **6**, 8245 (1994).
 - [12] J. P. Perdew and Y. Wang, Phys. Rev. B **45**, 13244 (1992).
 - [13] H. Jónsson, G. Mills, and K. W. Jacobsen, in *Classical and Quantum Dynamics in Condensed Phase Simulations*, edited by B. J. Berne, G. Ciccotti, and D. F. Coker (World Scientific, Singapore, 1998).
 - [14] H. Conrad, Progr. Mater. Sci. **26**, 123 (1981), pp. 131–134.
 - [15] T. Hahn, ed., *International tables for crystallography*, vol. A (Dordrecht: Kluwer Academic, 1996), 4th ed.
 - [16] A. L. Kutepov and S. G. Kutepova, Phys. Rev. B **67**, 132102 (2003).
 - [17] D. R. Trinkle, R. G. Hennig, S. G. Srinivasan, D. M. Hatch, M. D. Jones, H. T. Stokes, R. C. Albers, and J. W. Wilkins, Phys. Rev. Lett. **91**, 025701 (2003).
 - [18] S. P. Rudin, M. D. Jones, and R. C. Albers, cond-mat/0305331 (2003).